PERGAMON

Corrosion Science 44 (2002) 1287–1309

CORROSION SCIENCE

www.elsevier.com/locate/corsci

Application of EIS and SEM to evaluate the influence of pigment shape and content in ZRP formulations on the corrosion prevention of naval steel

J.R. Vilche [a], E.C. Bucharsky [b,*], C.A. Giúdice [c]

[a] *Instituto de Investigaciones Fisicoquímicas Teóricas y Aplicadas (INIFTA), Facultad de Ciencias Exactas, Universidad Nacional de La Plata, Sucursal 4, C.C.16, 1900 La Plata, Argentina*

[b] *Departamento de Ciencia y Tecnología, Universidad Nacional de Quilmes, Roque Saenz Peña 180, 1876 Bernal, Argentina*

[c] *Centro de Investigación y Desarrollo en Tecnología de Pinturas (CIDEPINT), calle 52 e/121 y 122, 1900 La Plata, Argentina*

Received 16 March 2001; accepted 14 September 2001

Abstract

The effects of pigment volume concentration and morphology of zinc particles employed in the formulation of zinc rich paints (ZRP) suitable for the corrosion protection of naval steel in sea water, have been investigated using electrochemical impedance spectroscopy combined with open circuit potential measurements and SEM micrograph analysis. Different ZRP samples were tested during exposure to artificial sea water for up to 70 days. The characteristics and properties of the naval steel/ZRP coating/sea water systems were determined from an impedance transfer function model which involves the reactions occurring at the metal/ZRP and ZRP/solution interfaces as well as diffusion processes through the active ZRP coating. Information concerning the influence of concentration and shape of the zinc pigment on the corrosion protective behaviour of ZRP coatings and on the exposure time dependence of the system parameters allowed to interprete the form in which the galvanic action and the barrier effect diminish progressively. The degree of rusting of the steel substrates as well as the blistering resistance of the formulated ZRP have been also evaluated according to conventional ASTM standards. © 2002 Elsevier Science Ltd. All rights reserved.

Keywords: Zinc rich paints; Impedance spectroscopy; Naval steel; Corrosion; Pigment shape

* Corresponding author.

0010-938X/02/$ - see front matter © 2002 Elsevier Science Ltd. All rights reserved.
PII: S0010-938X(01)00144-5

1. Introduction

Primers heavily pigmented with zinc dust have been extensively employed for the corrosion protection of steel structures [1,2]. Physicochemical properties as well as corrosion behaviour of zinc rich paints (ZRP) can be markedly affected by the shape and size of zinc dust, the pigment volume concentration (PVC) and the thickness of the dry film [3]. There is a critical value of PVC (CPVC) above which many of such dry film properties change abruptly, i.e. blistering and gloss decrease strongly whereas permeability and rusting increase dramatically [4,5].

Zinc dust consists of chemically pure metallic zinc, in the form of near spherical particles of selected sizes and size distribution [1]. It is important to note that the number of particles of various sizes must be adequate, so that the small particles slip in among the big ones and, accordingly, a large amount of zinc accumulates in the paint film. This dense packing promotes an effective contact between the zinc particles, making the paint film electrically conductive and enabling the generation galvanic cells which prevent the steel corrosion [2,6]. Furthermore, the dense packing of particles gives rise to coatings with an effective long lifetime and appropriate high mechanical resistance.

In general, most of the spherical zinc dust traditionally produced in USA is a relatively coarse dust, whose diameter averages from 6 to 8 μm [6]. Finer zinc dusts used in various countries are commonly denoted as: (i) fine zinc dust with an average particle size of about 4–5 μm; and (ii) superfine zinc dust, which exhibits particle sizes in the order 2–3 μm [6]. A small particle size could lead to ZRP which exhibits both effective electrical contacs and low current density with a proper distribution of zinc particles, although the large galvanic action could promote osmotic phenomena leading to an enhanced film blistering. On the other hand, steel plates protected with ZRP revealed more localized attack when zinc dust of the highest particle size is employed in the coating formulation [7].

The shape of pigment particles also contributes to remarkable differences in the specific effective area of metallic zinc during the corrosion process, so that lamellar zinc exhibits a higher surface area/weight ratio than that of spherical form [7,8]. Spherical zinc particles allow the protective current flux in a tangential form and, consequently, electrical contacts become limited to a few points. Nevertheless, the high density spherical zinc pigment provokes usually a fast sedimentation and strong agglomeration of particles which cannot be easily redispersed, even in the case of well formulated paints. This produces heterogeneous films since in some zones the PVC/CPVC ratio is higher than one, generating in this way a coating with poor mechanical properties and high porosity. Likewise, in the neighbouring areas with lower concentration of zinc particles the electrical contact appears to be insufficient to provide a satisfactory protective galvanic action to the underlying metallic structure. These subjects forced in the last years to examine the corrosion behaviour of lamellar zinc in primers to protect iron and steel substrates.

Results obtained from impedance spectroscopy data, open circuit corrosion potential measurements and visual assessments have been recently employed to evaluate the performance of ZRP during the exposure time to corrosive media [9–14].

The gradual deterioration of ZRP coatings during immersion in sea water was interpreted by employing either a simple Randles circuit [9,10], or the transmission line model [11,12], or transfer-function based reaction mechanisms developed to take into account the contributions of both anodic and cathodic processes at the corresponding open circuit corrosion potential which changes during exposure time to the aggressive electrolyte [13,14]. The analysis of impedance data used for the characterization of the corrosion performance of painted metals was critically discussed in several review papers [15–18].

The aim of the present work is to gain a deeper insigh on the corrosion protection behaviour of ZRP containing zinc particles of different morphology applied on naval steel, using electrochemical impedance spectroscopy (EIS) and open circuit corrosion potential measurements at different exposure times in artificial sea water complemented with SEM observations and accelerated tests in salt spray (fog) chamber and 100% relative humidity cabinet.

2. Experimental method

SAE 1020 (UNS G10200) steel plates $20 \times 8 \times 0.2$ cm^3 were used as metallic substrate. Metal surfaces were initially sandblasted to A Sa 2 1/2–3 degree (SIS Standard 05 59 00/67), degreased with vapour toluene, and finally coated with epoxypolyamine-amide ZRP; in all the cases panels were prepared in duplicate and stored seven days for curing at 20 ± 2 °C before beginning the tests. Some characteristics of the formulated ZRP and applied dry film thicknesses are assembled in Table 1. ZRP formulations included either lamellar zinc (samples L1 to L5) or spherical zinc (samples S1 to S8) as unique pigment; their physical properties are

Table 1
Characteristics of the different ZRP and Zn sprayed samples

Sample	Morphology of zinc dust	Thickness/μm (dry film)	PVC (%) (in dry film)
L1	Lamellar	40	50
L2	Lamellar	75	50
L3	Lamellar	80	50
L4	Lamellar	40	60
L5	Lamellar	60	60
S1	Spherical	50	50
S2	Spherical	40	60
S3	Spherical	60	60
S4	Spherical	70	60
S5	Spherical	80	60
S6	Spherical	35	70
S7	Spherical	45	70
S8	Spherical	65	70
Zn1	Spherical[a]	55	(100)
Zn2	Spherical[a]	75	(100)
Zn3	Spherical[a]	100	(100)

[a] Before application by thermal spray.

Table 2
Physical characteristics of metallic pigments

Zinc pigment	Spherical particle	Lamellar particle
Form	Powder	Powder
Colour	Gray	Dark gray
Odour	Odourless	Odourless
Density ($g\,cm^{-3}$)	7.1	7.1
Apparent density ($g\,cm^{-3}$)	2.4	1.0
Oil absorption (g/100 g)	13	21
Purity (%)	99.02	99.97

Table 3
Particle size distribution of lamellar zinc

Diameter (<μm)	% accumulate (lower)	% accumulate (bigger)	% difference
0.8	1.5	98.5	1.5
1.0	4.0	96.0	2.5
2.0	11.0	89.0	7.0
3.0	16.0	84.0	5.0
4.0	25.0	75.0	9.0
5.0	32.0	68.0	7.0
8.0	40.0	60.0	8.0
9.0	43.5	56.5	3.5
10.5	50.0	50.0	6.5
12.3	60.0	40.0	10.0
15.0	70.6	29.4	10.6
17.5	80.0	20.0	9.4
20.0	87.3	12.7	7.3
25.0	94.5	5.5	7.2
30.0	98.2	1.8	3.7
38.0	100.0	0.0	1.8

$D(10/90\%) = 1.9$ μm; $D(50/50\%) = 10.5$ μm; and $D(90/10\%) = 22.0$ μm.

given in Table 2 and the corresponding particle size distributions in Tables 3 and 4. The epoxy binder consisted of a base with a weight per epoxide about WPE ≈ 450, and a polyamine-amide hardener with an amine value in the range of 210–220. The solvent mixture, expressed as % w/w, was 42.7% xylene + 14.6% butanol + 42.7% oxygenated hydrocarbon. Clay modified with gel-like amines was added as rheological agent after finishing the pigment dispersion (1% w/w). A high speed agitation equipment was employed for pigment dispersion and mill base viscosity adjusted at this stage. Before primer application, the hardener was incorporated in the adequate ratio. For the sake of comparison, some steel samples were covered with thermal sprayed Zn (samples Zn1 to Zn3 in Table 1).

The ZRP dry film thickness was measured with an electromagnetic gauge employing bare sanded plates and standards of known thickness as reference. Potentials were measured and referred to in the text against a saturated calomel electrode (SCE). EIS measurements in the 3 mHz $\leqslant f \leqslant$ 65 kHz frequency range were performed in the potentiostatic mode at the corresponding corrosion potential attained

Table 4
Particle size distribution of spherical zinc

Diameter (<μm)	% accumulate (lower)	% accumulate (bigger)	% difference
0.5	1.5	98.5	1.5
0.8	3.0	97.0	1.5
1.0	5.0	95.0	2.0
2.0	12.0	88.0	7.0
3.0	16.0	84.0	4.0
4.0	32.0	68.0	16.0
5.0	45.0	55.0	13.0
6.0	55.0	45.0	10.0
7.0	67.0	33.0	12.0
8.0	76.0	24.0	9.0
9.0	82.0	18.0	6.0
10.0	88.0	12.0	6.0
11.0	90.0	10.0	2.0
12.3	93.0	7.0	3.0
15.0	96.0	4.0	3.0
17.5	98.5	1.5	2.5
20.0	99.0	1.0	0.5
38.0	100.0	0.0	1.0

$D(10/90\%) = 1.8$ μm; $D(50/50\%) = 5.4$ μm; and $D(90/10\%) = 11.0$ μm.

after different exposure times in artificial sea water using a frequency response analyzer and an electrochemical interface (Solartron, FRA 1250 and EI 1186, respectively) integrated with a PC system. The exposed geometrical area of samples was 1 cm^2. For impedance measurements, an activated Pt probe was coupled to the SCE through a 10 μF capacitor to reduce phase shift errors at high frequencies. Artificial sea water was prepared according to the ASTM Standard D 1141-90. Detailed descriptions of the experimental setup and data processing have been described elsewhere [18,19].

SEM observations were made using a Jeol T 100 microscope. Test samples were metallized with Au–Pd previous to the SEM observations. SEM data were used to characterize freshly prepared ZRP samples and the morphology and heterogeneites of corrosion products formed after different exposure times in sea water.

The standardized procedures ASTM B 117-85 (Salt Spray Chamber) and ASTM D 2247-94 (100% relative humidity cabinet) were also performed on the painted steel samples for comparing their results with the electrochemical ones. After these tests, the painted panels were assessed with the ASTM Standards D 1654-92 and D 714-87 in order to evaluate the degree of rusting and of blistering, respectively, in an attempt to correlate visual observations and electrochemical data.

3. Results and discussion

The exposure time dependence of the open circuit potential (E_{corr}) was used as a simple tool for the evaluation of corrosion protection by ZRP coatings due to their

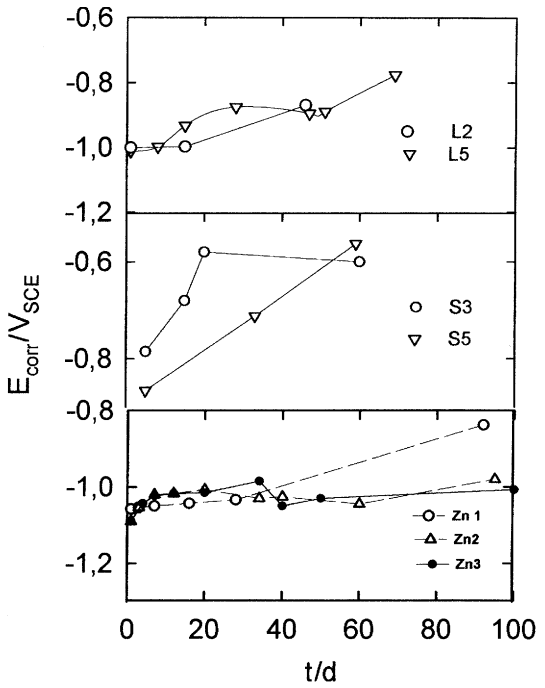

Fig. 1. Dependence of E_{corr} on exposure time in artificial sea water for lamellar and spherical ZRP coatings and thermal sprayed Zn coatings whose composition and thickness are indicated in Table 1.

conductive nature. Immediately after immersion of the painted steel panels in the electrolyte E_{corr} was about -1.10 V, a value which lies in the corrosion potential range of zinc electrodes in sea water. The time dependence of E_{corr} for the different tested samples, illustrates the corresponding galvanic protection supplied to naval steel substrates by paints loaded with zinc powder of different morphology exposed to artificial sea water for about 70 days (Fig. 1). This can be attributed to the relatively high permeability of the ZRP coatings. The change of the zinc particle morphology can be easily seen by comparison of top view SEM micrographs obtained from just cured ZRP dry films and after 70 days exposure to artificial sea water for both lamellar and spherical zinc particles.

The set of impedance spectra at different exposure times (Figs. 2–9) contains valuable information concerning the characteristic coating parameters as well as the kinetics and mechanism of the corrosion process going on extensively through pores and cracks in the ZRP films. In the range of high and intermediate frequencies Nyquist diagrams show a complex capacitive loop, which can be associated with the dynamic response of the active dissolution of zinc porous electrodes, while at the low frequencies the impedance behaviour resembles the contribution of a diffusion process. After a prolonged immersion time probable contributions to the impedance spectra at high frequencies due to the insulating characteristics of both binder and corrosion products covering the zinc particles as well as the steel surface, cannot be

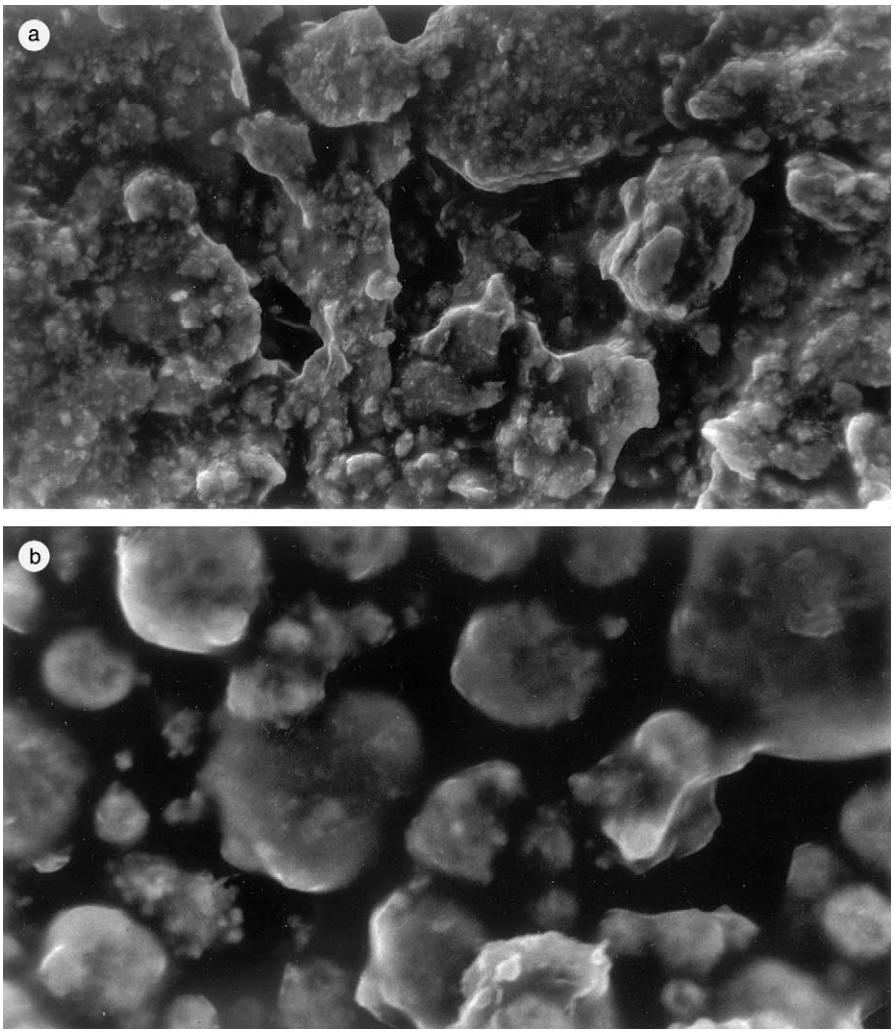

Fig. 2. Top view SEM micrographs of just cured ZRP: (a) lamellar zinc coating, PVC 50%, sample L3, (b) spherical zinc coating, PVC 60%, sample S5.

disregarded. Furthermore, a distribution of time constants should be also considered taking into account the profile of the frequency response like a depressed capacitive semicircle. Whenever the arc at the high frequencies can be related to the insulating properties of the coating, the length of its chord enables the estimation of the resistance of both binder and corrosion products. The diffusion impedance contribution detected in the low frequency region can be attributed to the transport process of reacting chemical species through the coating. Accordingly, the Warburg impedance Z_W for a diffusion process in a layer of finite thickness is given by the expression:

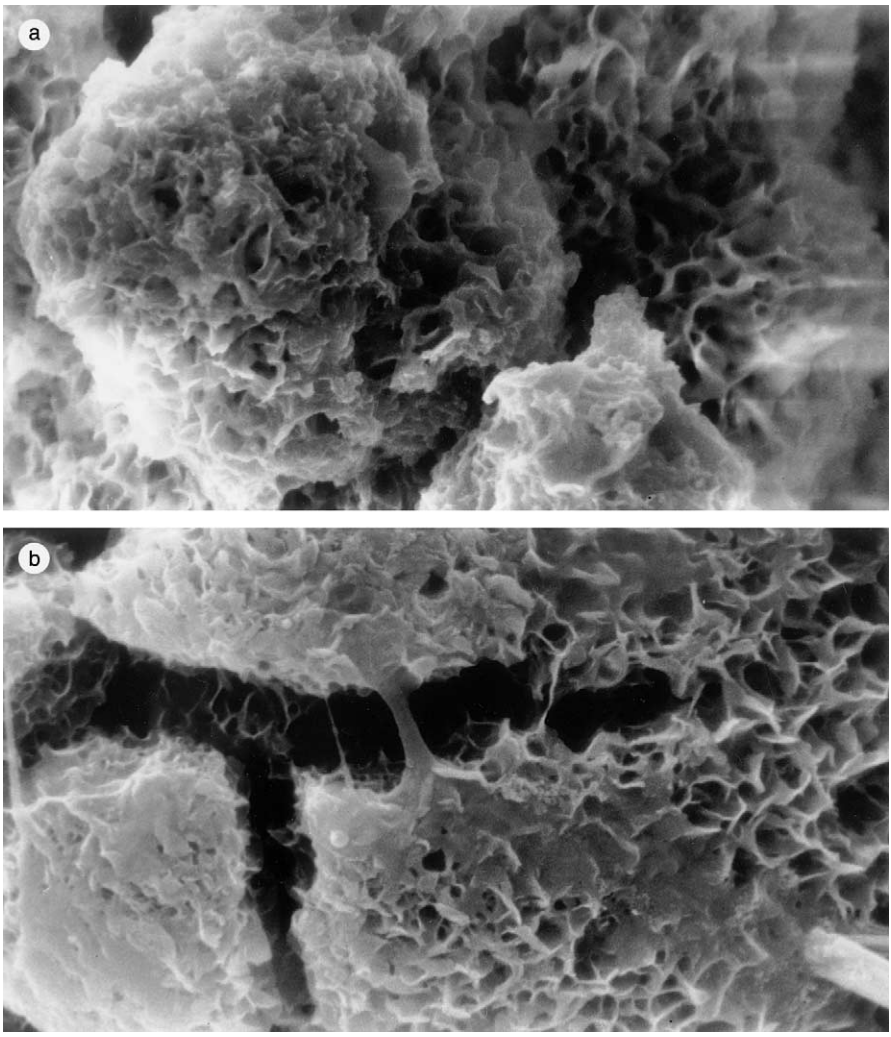

Fig. 3. Top view SEM micrographs of ZRP films exposed for 70 days to artificial sea water: (a) lamelar zinc coating, PVC 50%, sample L3, (b) spherical zinc coating, PVC 60%, sample S5.

$$Z_W(j\omega) = R_{D_0}(j\omega\delta^2/D)^{-0.5}\tanh(j\omega\delta^2/D)^{0.5} \quad (1)$$

where R_{D_0} denotes the $\omega \to 0$ limit of $Z_W(j\omega)$, δ is the thickness of the diffusion layer and D the diffusion coefficient. Thus, the lower the value of δ^2/D the sooner the diffusion tail, initially of 45° slope, will curve at decreasing frequencies towards the real axis.

The chord length pertaining to the high frequency loop observed in Nyquist diagrams tends to increase according to the exposure time in sea water. This effect can be related to the formation and accumulation of insoluble corrosion products within

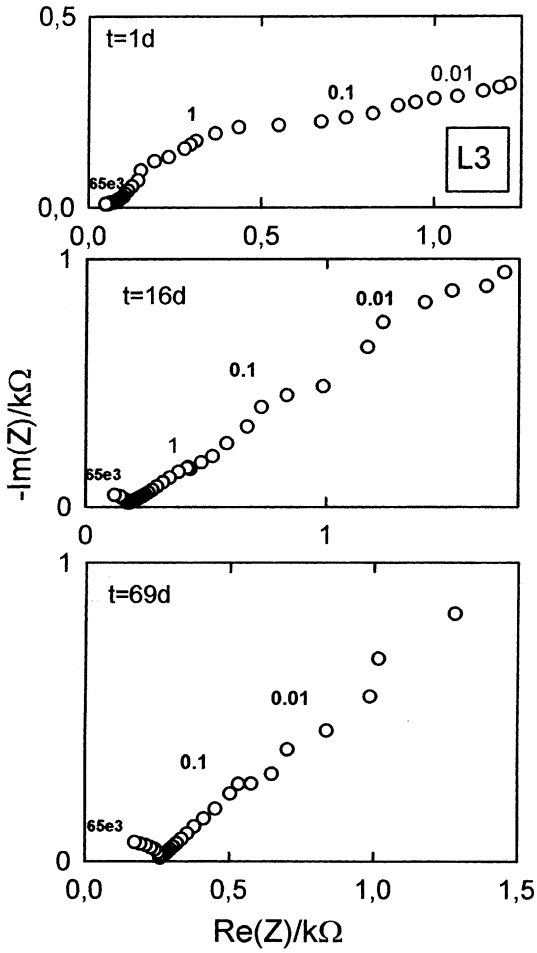

Fig. 4. Nyquist diagrams of sample L3 at different exposure times. Frequencies in Hz are marked.

the coating, whereas small amounts of pigment particles sustain the electrical contact among them as well as with the steel substrate. This is in agreement with the gradual change of the corrosion potential towards more positive values (see Fig. 1). The set of impedance diagrams of the system naval steel/ZRP/artificial sea water shown in Figs. 2–9 reveals that at constant ZRP thickness, the exposure time, the PVC and the zinc dust morphology affect strongly the frequency response of the paint films tested in this work. Changes in the coated naval steel/artificial sea water system seem to alter the dynamics of both zinc corrosion and rust formation reactions at relatively long exposure times.

A fairly good description of the experimental impedance diagrams was obtained in terms of transfer function analysis using non-linear fit routines (Figs. 10–14) according to the following total transfer function:

$$Z_T(j\omega) = R_\Omega + Z(j\omega) \tag{2}$$

where R_Ω is the solution resistance and $Z(j\omega)$ denotes the frequency response of the system, which can expressed by

$$[Z(j\omega)]^{-1} = [\mathrm{CPE}]^{-1} + \frac{R_C + R_{D_0}(j\omega\delta^2/D)^{-0.5}\tanh(j\omega\delta^2/D)^{0.5} + R_A}{\left[R_C + R_{D_0}(j\omega\delta^2/D)^{-0.5}\tanh(j\omega\delta^2/D)^{0.5}\right]R_A} \tag{3}$$

The transfer function described in Eqs. (2) and (3) corresponds to the dynamic behaviour of the equivalent circuit:

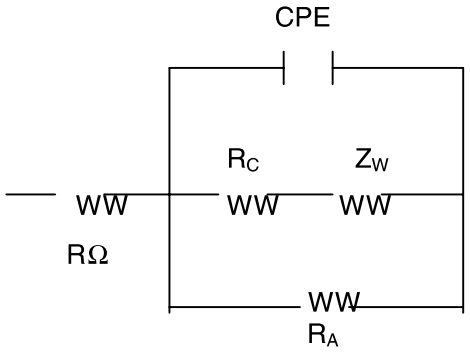

In Eq. (3), the constant phase element $\mathrm{CPE} = [C(j\omega)^{\alpha}]^{-1}$ involves a parameter α whose value was found to be in the range 0.4–0.6 for all the experiments. It should be noted that $\alpha = 0.5$ corresponds to the special case of porous electrodes and C the capacitance. The C values were calculated with Brug et al. sumptions [23]. The resistance R_C can be associated with the series combination of electrolyte resistance inside the pores and the charge transfer resistance of the oxygen reduction reaction (ORR). Therefore, a finite diffusion impedance was considered to account for the transport process involved in the cathodic partial reaction through the coating, and R_{D_0} the diffusion resistance as the $\lim \omega \to 0$ of $Z_W(j\omega) = R_{D_0}(j\omega l^2/D)^{-1/2}\tanh(j\omega l^2/D)^{1/2}$, l and D being the diffusion length and diffusion coefficient, respectively. On the other hand, R_A is related to the charge transfer resistance of the Zn dissolution process occurring in parallel with the ORR contribution [20,21].

The dependence of R_A, R_C, CPE and α on exposure time for the different samples are depicted in Fig. 15. The length of the high frequency arc chord is determined by the parallel connection of R_C associated with the series combination of the electrolyte resistance inside the pores and the charge transfer resistance of the process involving the ORR and R_A related to the charge transfer resistance of the zinc dissolution process. Similarly, at $\omega \to 0$ the real part of the impedance includes the sum of R_C and R_{D_0} contributions which are in parallel with R_A. Since R_A was found to be smaller than $R_C + R_{D_0}$ for all ZRP samples, the real part of the impedance at the lowest frequencies results mainly dominated by the anodic process. It is worth noting that

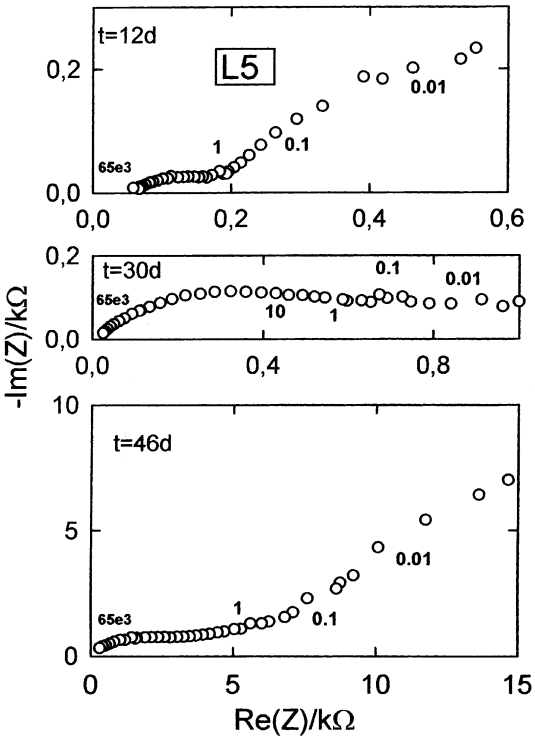

Fig. 5. Nyquist diagrams of sample L5 at different exposure times. Frequencies in Hz are marked.

the increase of the high frequency chord length according to the exposure time may be related to a rise in the electrolyte resistance inside the pores and to a decrease in the electrochemical active area generated by the accumulation of corrosion products. For the two types of zinc particle geometry the values of R_A and R_C increase with exposure time, this effect being more clearly observed with increasing film thickness. At comparable pigment content and film thickness, the values of polarization resistance $R_p = [R_A(R_C + R_{D_0})]/[R_A + R_C + R_{D_0}]$ with spherical zinc exceeded those corresponding to the lamellar shape. Therefore, the analysis of the whole set of data indicates that the best cathodic protection effect is given by all samples whose chemical composition included lamellar zinc particles. It should be noted that a fairly good cathodic protection effect was in action for L2 and L3 samples with a PVC value close to 50% and thickness in the order of 75–80 μm.

Taking into account the thickness of each lamellar as well as spherical ZRP coating, from the values of δ^2/D obtained for the different sample formulations one can estimate $D \approx (9 \pm 3) \times 10^{-6}$ cm^2 s^{-1}, a diffusion coefficient value which suggests that the mass transport phenomenon takes place in the solution within pores in the ZRP film. This diffusion process can be associated with the transport of dissolved oxygen from the coating/sea water interface to the bottom of pores, preceding the cathodic partial reaction of oxygen reduction. It is interesting to note that the

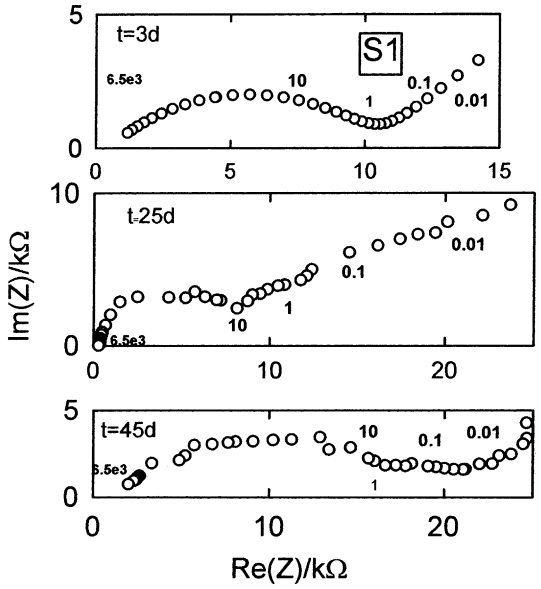

Fig. 6. Nyquist diagrams of sample S1 at different exposure times. Frequencies in Hz are marked.

diffusion coefficient of molecular oxygen in base media at 25 °C calculated from the Levich, Gregory and Riddiford and Newman equations yielded a value of about 1.1×10^{-5} $cm^2 s^{-1}$ [22].

Fig. 16 displays cross-section SEM micrographs corresponding to spherical ZRP film (sample S5) after 1 h immersion in artificial sea water. Zinc corrosion products are formed likely over the whole particles. Similar results were obtained for practically all samples independently of film thickness, indicating the good electrical contact between the zinc particles, particularly at PVC values close to the CPVC. This behaviour attained with the sample S5 remains up to the end of the experiment after 70 days exposure time. It is interesting to note that lamellar ZRP film (sample L3) with PVC/CPVC ratio approximately 1 also exhibited homogeneously distributed zinc corrosion products at the different film depths.

The decrease of C with increasing exposure time in artificial sea water can be related to the formation of corrosion products with dielectric properties, which diminishes the effective area of the zinc/solution interface and promotes a progressive loss of the electrical contact between zinc particles. The magnitude of changes seems to be the same in ZRP samples with comparable PVC and thickness values. In general, cross-section SEM micrographs reveal an increasing amount of zinc corrosion products as immersion time increases from 1 h to six days (Fig. 17), but after that no significant change was observed even after 70 days exposure time.

One characteristic of ZRP coatings usually used in aggressive environments for steel protection is that the optimum PVC seems to be higher than those values generally recommended in a typical anticorrosive paint. It is important to emphasize

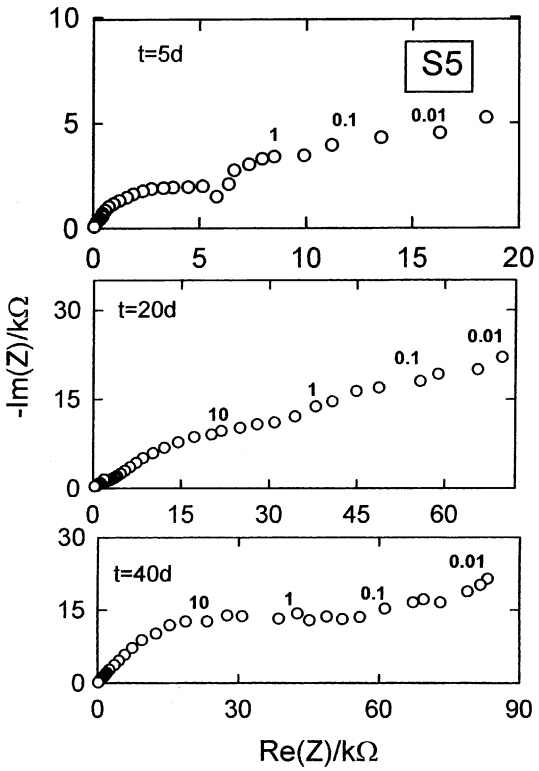

Fig. 7. Nyquist diagrams of sample S5 at different exposure times. Frequencies in Hz are marked.

that at constant dry film thickness the increase of PVC value diminishes R_p, but as PVC approaches the CPVC value R_p exhibits the opposite trend. This change correlates well with the expected corrosion behaviour taking into account that corrosion products accumulate on the zinc particles. It is noteworthy that in the case of ZRP including lamellar zinc particles the CPVC value appears to be close to 50% v/v, whereas it increases to about 60% v/v for spherical geometry. At the same thickness and PVC values, R_p is lower in coatings containing lamellar zinc. This fact can be attributed to the higher disponibility of metallic zinc as well as better cathodic protection. The exposure time dependence of kinetic parameters derived from the transfer function model which interpretes the experimental impedance data obtained with the different ZRP samples are in good agreement with the gradual changes of corrosion potential along exposure time in the aggressive electrolyte.

In the case of thermal sprayed Zn coatings, samples Zn1 to Zn3, the value of E_{corr} remained at high negative potentials, even after exposure times up to 100 days. This suggests an effective galvanic protection action. It is worthnoting that both R_A and R_C values diminished in the initial 10–15 days whereas those of C increased, while at longer exposure times the opposite trends were observed. This means, in

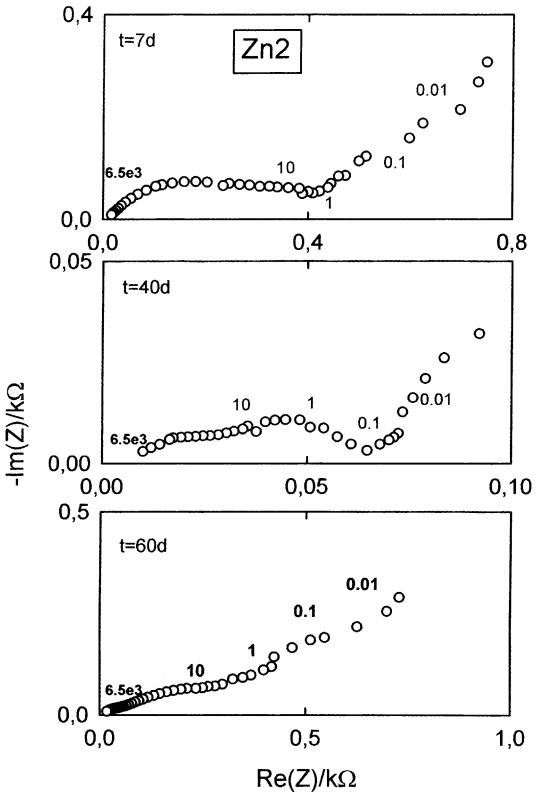

Fig. 8. Nyquist diagrams of sample Zn2 at different exposure times. Frequencies in Hz are marked.

principle, that after about 10–15 days in artificial sea water, the time dependences of kinetic parameters of thermal sprayed Zn coatings resemble those obtained for ZRP films.

According to the transfer function model given in Eqs. (2) and (3), it is possible to describe the relative impedance contribution of the different processes. On steel surface there are numerous very small areas of different potential so that two adjacent areas can generate a sort of electric cell using the steel substrate to provide direct electrical contact between these two points. At this stage no current can flow and hence no corrosion takes place because the electrical circuit is not closed. However, as soon as the electrolyte solution reaches these points the electrical circuit is completed and corrosion starts. At the more positive potential points the electrons react with dissolved oxygen yielding hydroxyl ions, which produces initially Fe(II)-hydroxide species and with further oxygen supply the typical rust. The corrosion process can be stopped by passing from an external source a current, whose value should be at least equal than the corrosion current, but in opposite direction to attain the cathodic protection phenomenon. The excellent corrosion prevention action of ZRP paints is due to the fact that the zinc dust can exclude the presence of

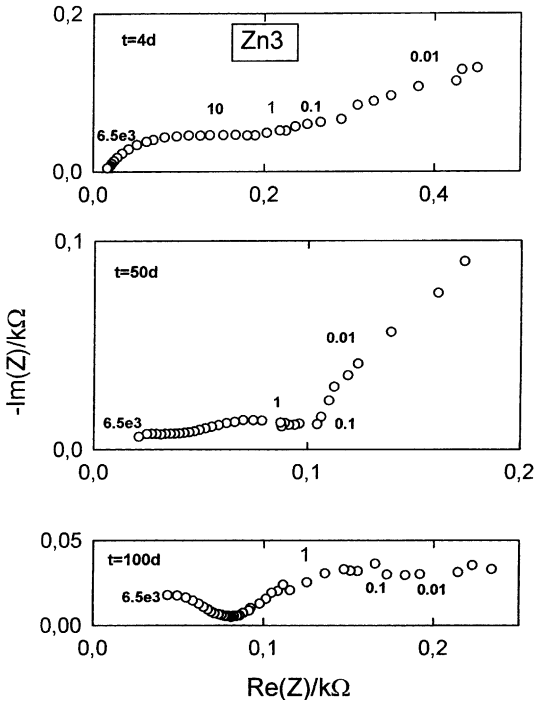

Fig. 9. Nyquist diagrams of sample Zn3 at different exposure times. Frequencies in Hz are marked.

oxygen at the steel surface and also protect cathodically the steel substrate at least in the initial stages of the exposure to aggressive media. With increasing exposure time both steel corrosion and formation of deposits on the zinc surface occur to appreciable extent. This behaviour indicates clearly that the necessary condition to provide the best protection against corrosion by means of zinc rich paints arises from an intimate contact with the steel substrate. In most cases this can only by achieved by blast cleaning the surface to bare metal and applying the ZRP coating immediately, before any contamination occurs.

Salt spray (fog) testing in line with ASTM B 117-85 (35 ± 1 °C, pH 6.5–7.2, $5 \pm 1\%$ w/w NaCl and continuous spraying) was performed for 2500 h. According to visual observations during testing, particularly in the nearest zone to scribe, the ZRP based on lamellar particles became more covered with zinc corrosion products than those based on spherical ones. This suggests that cathodic activity of the metallic powder exposed in the painted surface was greater in samples with lamellar zinc. It is interesting to note that in all cases the amount of basic compounds formed from pigment increased with increasing zinc content. Results corresponding to degree of rusting on painted steel surfaces are shown in Table 5, where the mean values of duplicate tests are included. The evaluation of degree of rusting was estimated employing the scale of ASTM D 1654-92 (method A for failure at scribe, while method

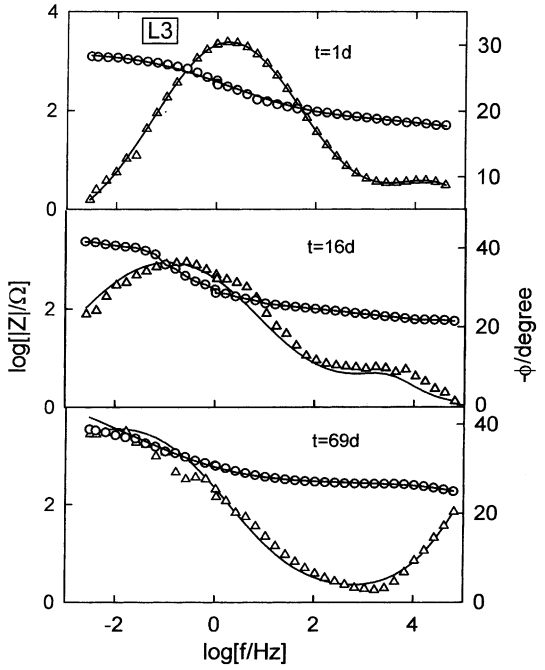

Fig. 10. Bode plots of sample L3 at different exposure times. Experimental (◯) and simulated (—) for the $|Z|$ vs $\log f$ and experimental (△) and simulated (—) for the phase (φ) vs $\log f$.

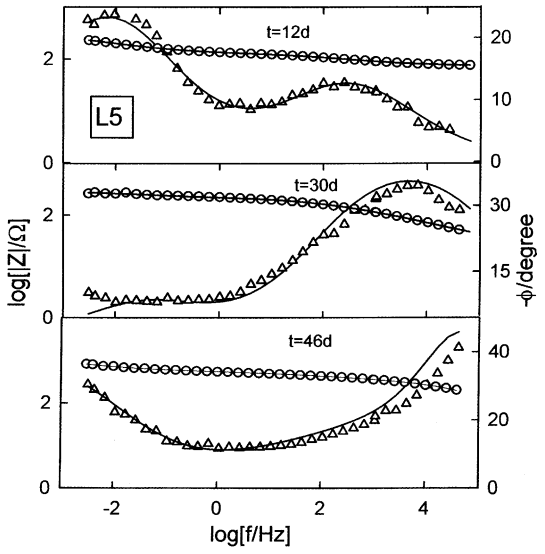

Fig. 11. Bode plots of sample L5 at different exposure times. Experimental (◯) and simulated (—) for the $|Z|$ vs $\log f$ and experimental (△) and simulated (—) for the phase (φ) vs $\log f$.

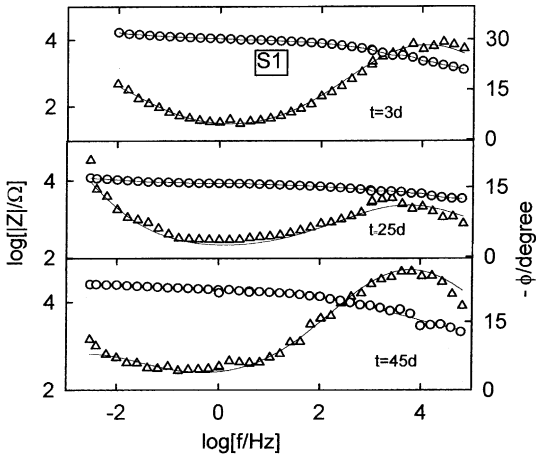

Fig. 12. Bode plots of sample S1 at different exposure times. Experimental (◯) and simulated (—) for the $|Z|$ vs log f and experimental (△) and simulated (—) for the phase (φ) vs log f.

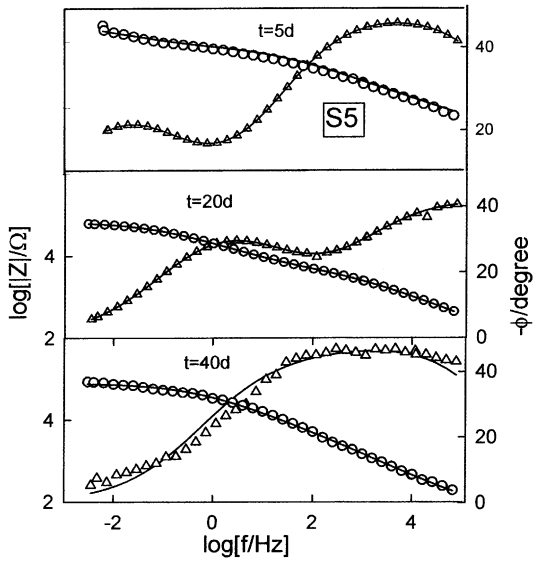

Fig. 13. Bode plots of sample S5 at different exposure times. Experimental (◯) and simulated (—) for the $|Z|$ vs log f and experimental (△) and simulated (—) for the phase (φ) vs log f.

B in the rest of the surface). Rating of failure at X-cut was determined according to the representative mean creepage from scribe; the value 10 defines a mean failure of 0 mm whereas 0 corresponds to at least 16 mm. In the unscribed area, failure is measured considering the surface fraction attacked by the aggressive medium; the scale ranges from 10 (no failure) to 0 (over 75% of the failed area).

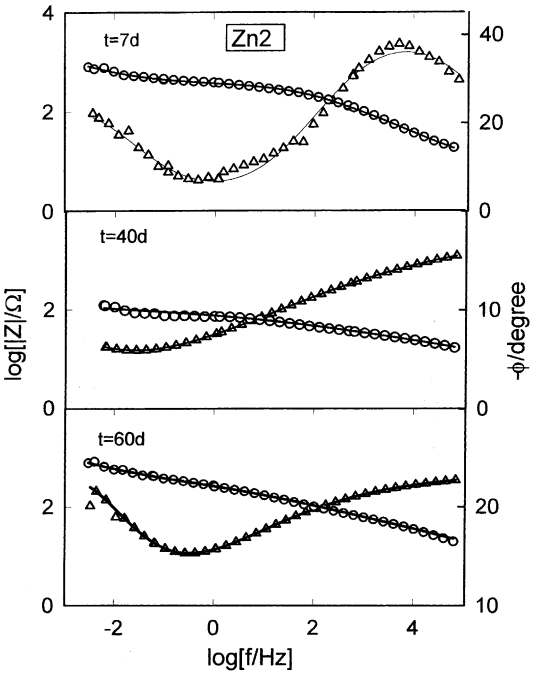

Fig. 14. Bode plots of sample Zn2 at different exposure times. Experimental (◯) and simulated (—) for the $|Z|$ vs log f and experimental (△) and simulated (—) for the phase (φ) vs log f.

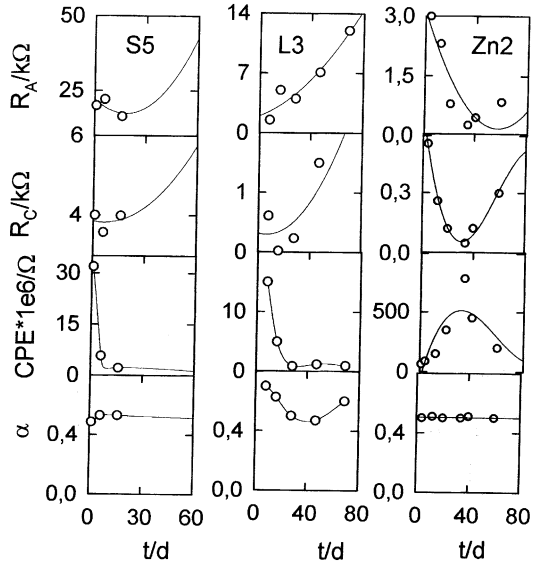

Fig. 15. Dependence of kinetic parameters R_A, R_C, C and α on exposure time in artificial sea water of samples S5, L3 and Zn2. Optimum fit results according to transfer function given in Eqs. (2) and (3).

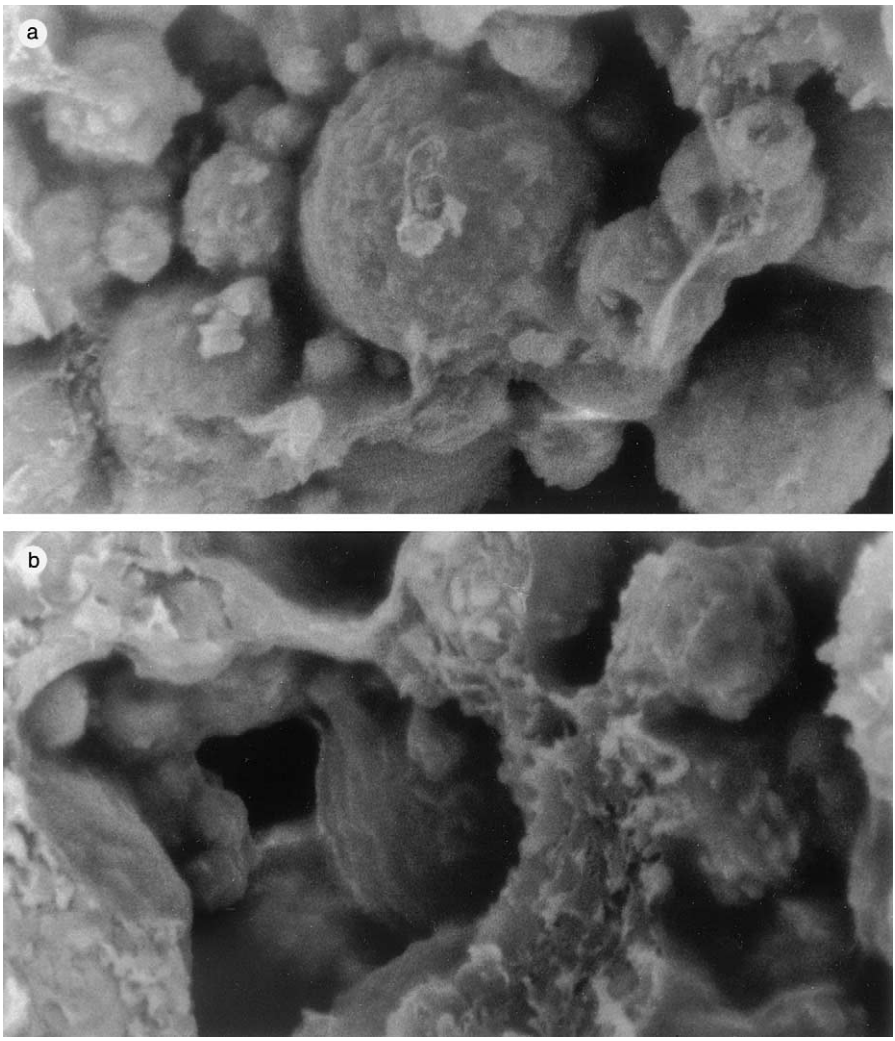

Fig. 16. Cross-section view SEM micrographs of spherical ZRP films, sample S5, exposed for 1 h to artificial sea water: (a) at about 5–6 μm from the steel/ZRP coating interface; (b) at about 55–57 μm from the steel/ZRP cating interface.

The analysis of data assembled in Table 5 gives rise to similar conclusions that those obtained from electrochemical methods. Therefore, the best corrosion protective behaviour in salt spray test for 2500 h was attained at PVC values about 50% for lamellar zinc (e.g. L3, 80 μm film thickness) and close to 60% for the spherical ones (e.g. S5, 80 μm film thickness), this means the formulation of films shown in Fig. 16. Besides, the assessment at both scribe and unscribe areas revealed an improvement of the corrosion protective behaviour of the coatings with lamellar zinc,

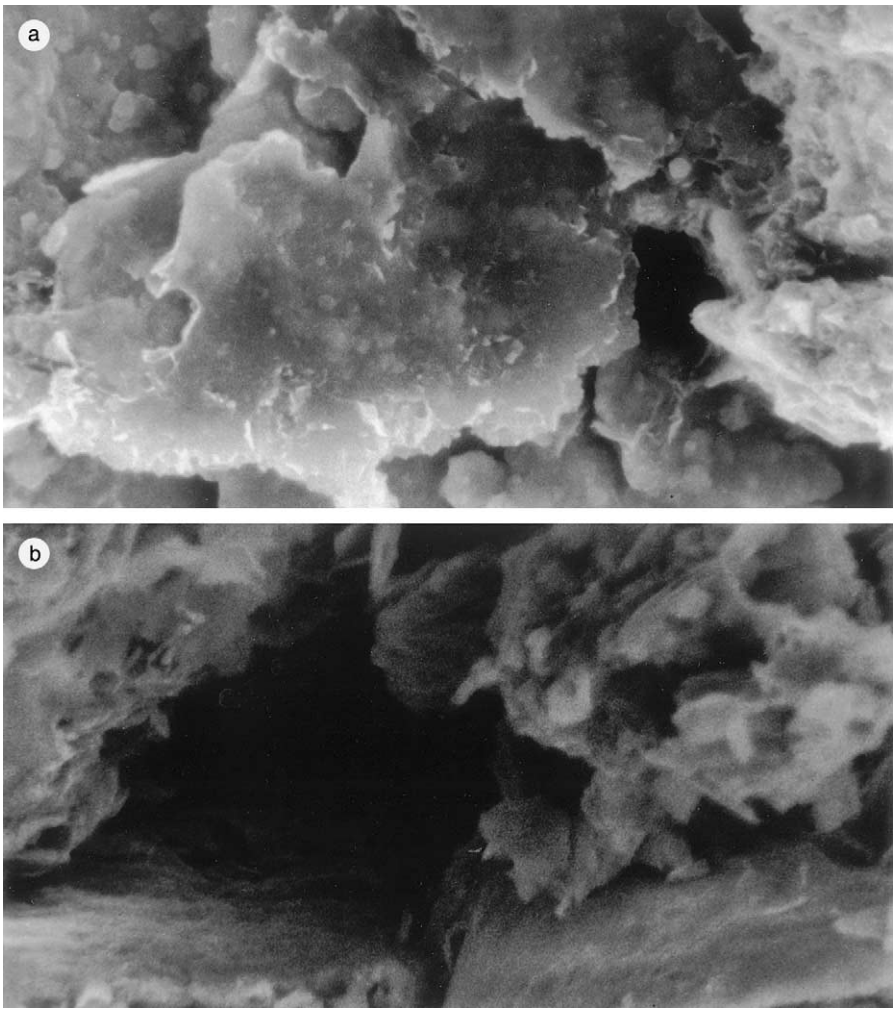

Fig. 17. Cross-section view SEM micrographs of lamellar ZRP films, sample L3, exposed to artificial sea water: (a) after 1 h exposure time, at about 20–22 μm from the steel/ZRP coating interface. (b) After six days exposure time, at about 20–22 μm from the steel/ZRP coating interface.

the best result being observed for a PVC value 50% and 80 μm film thickness. This can be explained owing to zinc corrosion products on spherical particles, which increase the electrical resistance of the protective system and decrease the amount of effective available zinc since the pigment particles could be electrically isolated between them as well as with the steel substrate. In conventional service conditions the dry film thickness usually applied permits enough water permeation leading to zinc corrosion, although the effective metal dissolution becomes hindered by the barrier effect due to zinc corrosion products. Consequently, the steel substrate exhibits a

Table 5
Degree of rusting, ASTM D 1654-92; salt spray (fog) testing, ASTM B 117-85, 2500 h

	Area	
	Scribed	Unscribed
Lamellar zinc rich primer		
L1	6	7–8
L2	9	10
L3	9–10	10
L4	5	4–5
L5	6	6
Spherical zinc rich primer		
S1	4	4–5
S2	4–5	5
S3	6–7	8
S4	7	9
S5	7–8	9–10
S6	3–4	4
S7	4	4–5
S8	7	7

more localizated attack. This gives support to interpretations of the lower corrosion control observed in the case of ZRP coatings with spherical dust, mainly when scribed areas are considered.

The accumulation of basic zinc compounds into the pores of the ZRP coating enhances both the barrier film effect and the protection action by chemical method due to a local alkalinization (unscribed area). A thicker dry film implies a higher metallic zinc content per unit steel area, allowing a longer corrosion control by the electrochemical method (scribed area). Therefore, ZRP film thicknesses in the order of 75–80 μm demonstrated better protection than those with 45–60 μm.

Results obtained from the 100% relative humidity test carried out according to ASTM D 2247-94 and evaluated in terms of degree of blistering by ASTM D 714-87 for 1000 h, are assembled in Table 6. Size of blistering is described in arbitrary units from 10 to 0, where 10 represents the absence of blistering, while the frequency of blistering is defined qualilatively as D (dense), MD (medium dense), M (medium) and F (few). Data given in Table 6 show an apparent higher tendency to blister in lamellar zinc coatings than in spherical ones, particularly at PVC values equal or

Table 6
Degree of blistering, ASTM D 714-87; 100% relative humidity chamber, ASTM D 2247-94, 1000 h

Lamellar zinc rich primer							
L1	L2	L3	L4	L5			
9-F	8-F	8-F	10	10			
Spherical zinc rich primer							
S1	S2	S3	S4	S5	S6	S7	S8
9-F	10	10	10	9-F	10	10	10

lower than the corresponding CPVC. No significant differences were detected at higher PVC, where the absence of blistering can be explained by considering that neither liquid nor gas generated bubbles from the paint film/steel interface due to an enhanced film permeability. The higher tendency to form soluble corrosion products in lamellar zinc containing films allows to interprete their lower blistering resistance detected in the 100% relative humidity test (osmotic blistering).

It is worth noting that after six month storage, lamellar zinc incorporated to epoxy base showed very low sedimentation, and adding the curing agent the primer can be applied with only a previous light stirring. On the other hand, spherical zinc primers, for the quoted elapsed time in can, displayed a heavy pigment settlement and, consequently, a very difficult handly redispersion.

4. Conclusions

EIS is an useful tool in the assessment of the protective behaviour of ZRP organic coatings formulated with different zinc morphology and PVC. Impedance spectra can be interpreted using a non-linear fit routine according to transfer function analysis. ZRP epoxypolyamine-amide coatings employed in this work tend to act as porous electrodes probably because most of the steel surface and reactive pigment particles maintain the electrical contact among them. The change of capacitance values, the increase of the resistances R_A, R_C, and the appearance of a diffusion process with increasing exposure time, can be attributed to the progressive disconnection of the pigment particles taking place simultaneously with the gradual thickening of the zinc corrosion product layer on the same particles.

The relative duration of the cathodic protection effect was practically similar for samples containing lamellar zinc at PVC values close to the CPVC when the dry film thickness exceeded 60 μm, whereas those coatings formulated with spherical zinc exhibited an effective time for cathodic protection slightly longer at PCV about 60% for dry film thickness higher than 60 μm. It is noteworthy that the best corrosion protective results at the end of the test, including galvanic action and barrier effect, were obtained using samples containing lamellar zinc particles under the same experimental conditions. Data obtained from both EIS and corrosion potential measurements as well as visual observations demonstrate that ZRP films containing a PVC level higher than the corresponding CPVC value deteriorate relatively faster in artificial sea water than those coatings formulated at zinc particle contents close to the CPVC.

The dependence of both kinetic parameters and open circuit corrosion potential on the exposure time in sea water correlates well with the gradual ZRP deterioration. Changes of the ZRP behaviour and steel corrosion degree during the exposure time agree with the system and reaction modelling derived from EIS data.

Lamellar zinc primers showed a low value of the effective PVC, so that about 50% was the best and consequently close to the estimated CPVC. For spherical zinc dust, it seems to be a little higher (approximately 60%). The particles of lamellar zinc have an increased surface area for a given weight, that is a higher value of specific area

than the spherical dust. Consequently, lamellar zinc used as pigment could lead to films with a higher electrical contact and with better superficial distribution of protective current. Then, the particle shape of lamellar zinc may be the responsible of the high efficiency performed in salt spray (fog) chamber for 2500 h.

Acknowledgements

This research project was financially supported by the Consejo Nacional de Investigaciones Científicas y Técnicas (CONICET) and the Comisión de Investigaciones Científicas de la Provincia de Buenos Aires (CIC).

References

[1] C.G. Munger, Corrosion Prevention by Protective Coatings, third ed., NACE, Houston, TX, 1986.
[2] H. Leidheiser (Ed.), Corrosion Control by Organic Coatings, NACE, Houston, TX, 1981.
[3] E. Montes, J. Coat. Techn. 65 (821) (1993) 79.
[4] W.K. Asbeck, M. van Loo, Ind. Eng. Chem. 41 (1949) 1470.
[5] G.P. Bierwagen, J. Paint Technol. 44 (574) (1972) 46.
[6] A.S. Kafka, Cap. V 'Zinc pigment', in: T.C. Patton (Ed.), Pigment Handbook, vol. I, 1973, pp. 819–832.
[7] B. del Amo, C.A. Giúdice, Am. Paint Coat. J. 76 (1991) 36.
[8] C.H. Hare, S.J. Wright, J. Coat. Technol. 54 (693) (1982) 65.
[9] S. Feliu, R. Barajas, J.M. Bastidas, M. Morcillo, J. Coat. Technol. 61 (775) (1989) 63, 69.
[10] R.A. Armas, C.A. Gervasi, A.R. Di Sarli, S.G. Real, J.R. Vilche, Corrosion 48 (1992) 379.
[11] S.G. Real, A.C. Elías, J.R. Vilche, C.A. Gervasi, A. Di Sarli, Electrochim. Acta 38 (1993) 2029.
[12] X. Novoa, M. Izquierdo, P. Merino, L. Espada, Mater. Sci. Forum 111–112 (1995) 257.
[13] C.A. Gervasi, A.R. Di Sarli, E. Cavalcanti, O. Ferraz, E.C. Bucharsky, S.G. Real, J.R. Vilche, Corros. Sci. 36 (1994) 1963.
[14] C.M. Abreu, M. Izquierdo, M. Keddam, X. Nóvoa, H. Takenouti, Electrochim. Acta 41 (1996) 2405.
[15] F. Mansfeld, M. Kendig, in: C. Haynes, R. Baboian (Eds.), Electrochemical Impedance Test of Protective Coatings, ASTM Publication STP 866, Philadelphia, 1985, p. 122.
[16] G.W. Walter, Corros. Sci. 26 (1986) 681.
[17] F. Mansfeld, J. Appl. Electrochem. 25 (1995) 187.
[18] E.C. Bucharsky, S.G. Real, J.R. Vilche, Corros. Rev. 14 (1996) 15.
[19] E.B. Castro, S.G. Real, R.H. Milocco, J.R. Vilche, Electrochim. Acta 36 (1991) 117.
[20] E.C. Bucharsky, S.G. Real, J.R. Vilche, J. Braz, Chem. Soc. 6 (1995) 39.
[21] C.A. Gervasi, A.R. Di Sarli, E.C. Bucharsky, S.G. Real, J.R. Vilche, Mater. Sci. Forum 192–194 (1995) 357.
[22] L.P. Kholpanov, Russ. J. Phys. Chem. 41 (1967) 1085.
[23] G.I. Brug, A.L.G. Van Den Eeden, M. Sluyters-Rehbach, J.H. Sluyters, J. Electroanal. Chem. 176 (1984) 275.